frontiers in Marine Science

ORIGINAL RESEARCH
published: 25 January 2022
doi: 10.3389/fmars.2021.778335

Impact of Decadal Trends in the Surface Climate of the North Atlantic Subpolar Gyre on the Marine Environment of the Barents Sea

Vimal Koul[1,2]*, *Sebastian Brune*[2], *Johanna Baehr*[2] *and Corinna Schrum*[1,2]

[1] Helmholtz Zentrum Hereon, Institute of Coastal Systems, Geesthacht, Germany, [2] Institute of Oceanography, Center for Earth System Research and Sustainability, Universität Hamburg, Hamburg, Germany

The Barents Sea is a key region in the Earth System and is home to highly productive marine resources. An integrated approach for strategic sustainable management of marine resources in such shelf-sea marine ecosystems requires, among many other aspects, a robust understanding of the impact of climate on local oceanic conditions. Here, using a combined observational and modelling approach, we show that decadal climatic trends associated with the North Atlantic Subpolar Gyre (SPG), within the period 1960–2019, have an impact on oceanic conditions in the Barents Sea. We relate hydrographic conditions in the Barents Sea to the decadal variability of the SPG through its impact on the Atlantic Inflow via the Faroe-Shetland Channel and the Barents Sea Opening. When the SPG warms, an increase in the throughput of subtropical waters across the Greenland-Scotland Ridge is followed by an increase in the volume of Atlantic Water entering the Barents Sea. These changes are reflected in pronounced decadal trends in the sea-ice concentration and primary production in the Barents Sea, which follow the SPG after an advective delay of 4–5 years. This impact of the SPG on sea-ice and primary production provides a dynamical explanation of the recently reported 7-year lagged statistical relationship between SPG and cod (*Gadus morhua*) biomass in the Barents Sea. Overall, these results highlight a potential for decadal ecosystem predictions in the Barents Sea.

Keywords: Barents Sea, Subpolar Gyre, Atlantic Inflow, marine ecosystems, decadal variability

OPEN ACCESS

Edited by:
Oeystein Skagseth, Norwegian Institute of Marine Research (IMR), Norway

Reviewed by:
Manuel Bensi, Istituto Nazionale di Oceanografia e di Geofisica Sperimentale, Italy
Anne Britt Sando, Norwegian Institute of Marine Research (IMR), Norway

***Correspondence:**
Vimal Koul
vimal.koul@hereon.de

Specialty section:
This article was submitted to Physical Oceanography, a section of the journal Frontiers in Marine Science

Received: *16 September 2021*
Accepted: *20 December 2021*
Published: *25 January 2022*

Citation:
Koul V, Brune S, Baehr J and Schrum C (2022) Impact of Decadal Trends in the Surface Climate of the North Atlantic Subpolar Gyre on the Marine Environment of the Barents Sea. Front. Mar. Sci. 8:778335. doi: 10.3389/fmars.2021.778335

1. INTRODUCTION

The Subpolar Gyre (SPG) of the North Atlantic is a cyclonically circulating oceanic gyre that exhibits pronounced decadal-to-multidecadal variability in its properties (Delworth et al., 1993; Marshall et al., 2001; Böning et al., 2006; Born and Mignot, 2012). Over the last sixty years, periods of strong decadal trends in surface temperature of the SPG (-60:10 °E, 50:62 °N) have been observed—cooling in the 1960s, the warming in the 1990s and the recent cooling in the 2000s (Dickson et al., 1988; Bersch et al., 2007; Reverdin, 2010; Robson et al., 2016; Piecuch et al., 2017; Holliday et al., 2020). The SPG has also been widely implicated as the source of large-scale changes in the subpolar marine environment (Hátún et al., 2009, 2016), and is thought to influence the properties of the Atlantic Inflow to the Nordic Seas (Hátún et al., 2005; Koul et al., 2020; Asbjørnsen et al., 2021). Recently, the SPG was also shown to impart decadal predictability to the cod (*Gadus morhua*) stock

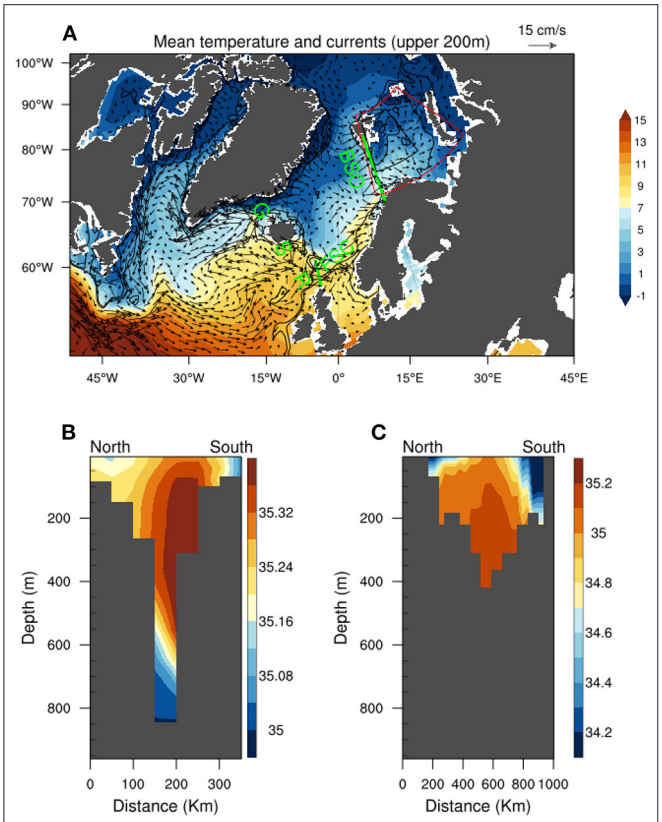

FIGURE 1 | (A) Mean (1960:2019 average) temperature and currents (upper 200 m) in the subpolar North Atlantic from the assimilation experiment. The black lines show 200 m and 500 m isobaths. Mean salinity at the hydrographic section at **(B)** Faroe Shetland Channel (FSC) and **(C)** Barents Sea Opening (BSO). The sections are shown as green lines in **(A)**. The Barents Sea regions analyzed in this study are defined as the black box (for wind stress curl) and red box (for Atlantic Water volume) in **(A)**.

in the Barents Sea (Årthun et al., 2018; Koul et al., 2021). However, the underlying dynamical mechanisms linking the decadal trends in the SPG to the Barents Sea, via the Faroe-Shetland Channel (FSC) and the Barents Sea Opening (BSO) (**Figure 1**), and their impact on local marine environment remained incompletely understood.

The Barents Sea is a highly productive shelf sea and is open to the influence of the Atlantic Ocean through the southwest. It acts as a transition zone for the warm and saline Atlantic Water headed toward the Arctic Ocean and plays an important role in the transformation of Atlantic water masses (Smedsrud et al., 2013). Over the past decades, the climate of the Barents Sea has undergone a dramatic change. The sea-ice area in the Barents Sea has declined by more than 50% in the last 30 years (Årthun et al., 2012), and the area occupied by the warm and saline Atlantic Water has nearly doubled (Dalpadado et al., 2012; Oziel et al., 2017). Observations also reveal large shifts in fish communities resulting from the "Atlantification" [increase in Atlantic Water transport into the Barents Sea and subsequent decline in sea-ice extent, see Årthun et al. (2012)] of the Barents Sea (Fossheim et al., 2015). While the greenhouse gas warming is an important factor in driving these observed long term changes in the Barents Sea, an important role of the variability originating in the subpolar North Atlantic in driving decadal to multi-decadal changes in the Barents Sea has also been well recognised (Levitus et al., 2009; Yashayaev and Seidov, 2015; Årthun et al., 2019).

An important source of climate and ecosystem variability in the Barents Sea is the inflowing Atlantic Water at its southwestern entrance, i.e., at the BSO (Ottersen and Stenseth, 2001; Smedsrud et al., 2010). An increase in the volume flux of the Atlantic Water is positively correlated with the temperature of the Barents Sea (Oziel et al., 2017). At interannual to decadal timescales (1–10 years), the variability in the volume flux of Atlantic Water at the BSO is, in-turn, largely driven by atmospheric variability associated with the North Atlantic Oscillation (NAO, Ingvaldsen et al., 2003; Sandø et al., 2010). For example, periods of a positive NAO are associated with enhanced southwesterly winds which increase the volume flux of Atlantic Water and plankton into the Barents Sea (Drinkwater et al., 2003). However, the relationship between large scale atmospheric winds associated with the NAO and the volume flux of Atlantic Water into the Barents Sea is non-stationary (Smedsrud et al., 2013), and there are periods when the role of local wind forcing dominates (Orvik and Skagseth, 2003; Lien et al., 2017; Muilwijk et al., 2018).

Apart from the variability in the volume flux of the Atlantic Water at the BSO, a change in Barents Sea temperature can occur due to a change in temperature of inflowing Atlantic Water. In this case as well, the NAO can influence the temperature of the inflowing water through its impact on the width of the Norwegian Atlantic Current and thereby controlling how much heat this current exchanges with the atmosphere (Ådlandsvik and Loeng, 1991). Another source of changes in the temperature of inflowing Atlantic Water is the thermohaline anomalies originating in the subpolar North Atlantic which are known to propagate downstream toward the Nordic Seas (Holliday et al., 2008; Yashayaev and Seidov, 2015). On multidecadal timescales (>50 years), the climate of the Barents Sea varies with the Atlantic Multidecadal Variability (AMV, Levitus et al., 2009; Yashayaev and Seidov, 2015), a manifestation of the rise and fall of North Atlantic surface temperatures. Embedded in such variability is decadal to multidecadal variability (also called inter-decadal timescales) associated with the SPG, the impact of which is the focus of the present study.

At decadal to multi-decadal time scales (10–20 years), the origin and propagation of heat and freshwater anomalies into the Nordic Seas and further downstream toward the Arctic has been investigated in observations and model simulations (Glessmer et al., 2014; Årthun and Eldevik, 2016; Langehaug et al., 2019). A consistent view emerging from these studies is that the variability in large scale oceanic circulation in the subpolar North Atlantic is the source of oceanic anomalies propagating into the Nordic Seas and further downstream. However, in light of the reported advective lags, it is not known whether and to what extent the observed hydrographic and biogeochemical anomalies in the Barents Sea follow the decadal trends in the surface climate of the SPG.

In this article, we investigate SPG-driven dynamical links between the variability in the Atlantic Inflow at the FSC and at the BSO extending back to 1960, and the subsequent impact of such variability on the volume of Atlantic Water and the sea-ice in the Barents Sea. We assess three dominant decadal trends in the surface temperature of the SPG whose impact on the Barents Sea is likely to be pronounced. Our results illustrate that the SPG signal can be traced in sub-surface properties at the BSO, and we hypothesise that by modulating the throughput of the Atlantic Water, the SPG causes variability in Atlantic Water volume in the Barents Sea. Our results also illuminate the dynamical basis for the recently reported statistical relationship between the SPG and cod biomass in the Barents Sea (Årthun et al., 2018; Koul et al., 2021). Changes in Atlantic Water volume have an impact on cod biomass through changes in sea-ice extent and primary production in the Barents Sea.

2. MATERIALS AND METHODS

The available oceanic observations in the subpolar North Atlantic cover important hydrographic sections but do not provide a continuous spatiotemporal record of surface and sub-surface temperature, salinity, and velocity fields extending back to 1960s. In this respect, we carry a data assimilation experiment with an Earth System Model that combines available atmospheric and oceanic observations and model output to provide a continuous spatiotemporal record over the past 60 years. The climatological temperature, salinity and velocity fields from this data assimilation experiment over the regions of interest are shown in **Figure 1** and **Supplementary Figure 1**.

Time series of surface temperature over the SPG (area averaged over -60:-10 °E, 50:62 °N) and BSO (area averaged over 10:25 °E, 70:78 °N) from this assimilation experiment compare very well with observations (Koul et al., 2021) and are analyzed in the present work. Additionally, satellite observations of sea-ice concentration (Meier et al., 2021, data retrieved from https://nsidc.org/data/g02202/versions/4/) and chlorophyll-derived net primary production (Behrenfeld and Falkowski, 1997, data retrieved from http://orca.science.oregonstate.edu/1080.by.2160.monthly.hdf.vgpm.m.chl.m.sst.php) are also analyzed to complement the results from the assimilation experiment. The time series of the TSB of Northeast Arctic Cod is obtained from the ICES Arctic Fisheries Working Group's report (http://doi.org/10.17895/ices.pub.6050).

We also analyze the time series of the annual mean volume transport through the FSC and the BSO (see **Figure 1** for the location of these sections). We define "total volume transport" as the volume transport (Sv, 1 Sv $= 10^6$ m^3 s^{-1}) of all eastward (u>0) flowing waters in the entire water column. The 1960–2019 mean total volume transport is about 5.9 Sv at the FSC and 3.65 Sv at the BSO which is larger than the observational estimates of 4 Sv at the FSC (Berx et al., 2013) and 1.8 Sv at the BSO (Skagseth et al., 2008) but within the range of estimates from other global ocean models (Ilıcak et al., 2016). We distinguish the total volume transport from the "Atlantic Inflow," which is defined as the volume transport of all eastward (u>0) flowing waters in the entire water column with T>8.5 °C, S>35.25 at the FSC, and T>5.5 °C, S>35.0 at the BSO. The Atlantic Inflow is essentially the warm and saline part of the total volume transport. Within the Barents Sea, the spatial extent of the volume of the warm and saline water is also analyzed. We define "Atlantic Water" as water with T>3 °C and S>34.8 (Oziel et al., 2016).

2.1. Model

The Max Planck Institute Earth System Model (MPI-ESM) is a global Earth system model, and is used in its low resolution (LR) setup in the present study (hereafter MPI-ESM-LR). The ocean general circulation component of MPI-ESM-LR, the Max Planck Institute Ocean Model, MPIOM (Jungclaus et al., 2013), is a free surface model with primitive equation solved on an Arakawa C-grid, and with hydrostatic and Boussinesq approximations. It has a total of 40 z-levels in the vertical and the surface layer thickness is 12 meters. Formulations by Pacanowski and Philander (1981) are followed for vertical mixing and diffusion, and tracer transport is parameterized following Gent et al. (1995). Statically unstable flow over sills and shelves is represented by a slope-convection scheme (Marsland et al., 2003).

The MPIOM setup used in the study has a rotated grid configuration (GR15) for which the singularity at the North Pole is replaced over Greenland. This has the advantage that horizontal resolution is enhanced north of 50°N, reaching 15 KM near Greenland. Otherwise, the nominal horizontal resolution of MPIOM in LR setup is 1.5 degrees. Embedded in MPIOM is also the ocean biogeochemistry component, the Hamburg Ocean Carbon Cycle model, HAMOCC (Ilyina et al., 2013). Among other processes, HAMOCC incorporates phosphate and oxygen cycles, and defines marine food web based on nutrients, phytoplankton, zooplankton, and detritus (NPZD) based approach.

The atmospheric general circulation component of MPI-ESM-LR is the European Center-Hamburg model, ECHAM, (Stevens et al., 2013). In MPI-ESM1.2-LR, the ECHAM is run at a horizontal resolution of T63 and with 47 vertical levels, the model top being at 0.0 1hPa. The land surface-atmosphere interactions are simulated by the land vegetation module, JSBACH (Reick et al., 2013) which is embedded in ECHAM. A land hydrology module which contains a river-routing scheme is used for interactive simulation of river runoff (Hagemann and Gates, 2003), MPIOM receives the fresh water fluxes due to river runoff as part of the precipitation field from ECHAM.

2.2. Model Experiment

We analyze a data assimilation experiment (1960–2019) carried out with MPI-ESM-LR using an oceanic ensemble Kalman filter (EnKF) and atmospheric nudging. The oceanic EnKF in MPI-ESM-LR (Brune et al., 2015; Brune and Baehr, 2020) assimilates monthly profiles of temperature and salinity from EN4 (Good et al., 2013). Simultaneously, atmospheric vorticity, divergence, temperature, and surface pressure are nudged to ERA40/ERAInterim re-analyses (Dee et al., 2011). It should be noted that neither sea surface temperature from satellite observations nor atmospheric temperature below 900 hPa are assimilated in order to allow for a model-consistent assimilation

across the atmosphere-ocean boundary. The assimilation experiment uses observed solar irradiation, volcanic eruptions, and atmospheric greenhouse gas concentrations (SSP2-4.5 concentrations from 2015 onward) as boundary conditions, taken from CMIP6 (Eyring et al., 2016).

2.3. Trend Analysis and Statistical Significance

We compute linear trends over three periods of 10-years each except for sea-ice concentration and primary production wherein only 9 years from the last decade are considered after taking into account the advective delays from the SPG to the Barents Sea (detailed explanation is provided in the results and discussion sections). The statistical significance of the trend is calculated using a bootstrap approach wherein robust properties of a statistic (in this case the linear trend) are computed through random sampling and replacement to generate a distribution of the statistic. The confidence interval is taken as the 90% range (5^{th} to 95^{th} percentile) of this distribution. Our null hypothesis is that of a zero trend, and we fail to reject the null hypothesis if zero lies within the confidence intervals. Other non-parametric estimates of the linear trend and their statistical significance such as the Theil-Sen estimate of linear trend and the Mann-Kendall test were also evaluated (figures not shown). Except for the statistical significance of the 9-year trends for sea-ice and primary production (in our analysis, at-least 10-years are required for the Mann-Kendall test), our results are robust to these different estimates of decadal trends.

2.4. Correlations and Statistical Significance

All the correlations presented in this article are calculated from detrended time series (linear trend over 1960–2019 is removed). The non-detrended time series are presented in the main text. The statistical significance of correlation is assessed using a two tailed *t*-test. To account for the autocorrelation in the time series, the degrees of freedom is calculated by taking into account the lag-1 autocorrelation of the time series (Bretherton et al., 1999).

3. RESULTS

Decadal trends can be identified in surface temperature (T) and salinity (S) of the SPG over the past sixty years (**Figure 2**). Three decades clearly stand out when the trends were strong: (a) the cooling from 1966 to 1975, coinciding with the "great salinity anomaly" (Dickson et al., 1988), (b) the warming and salinification from 1996 to 2005, coinciding with a marked shift in the NAO phase in the winter of 1995/96 (Bersch et al., 2007), and (c) the cooling from 2006 to 2015, when the largest freshening event in more than a century was observed (Holliday et al., 2020). The basin-wide extent of the spatial patterns of these decadal trends and the concurrence of the periods of cooling and freshening as well as those of warming and salinification suggest that variability in large scale ocean circulation is involved (Piecuch et al., 2017; Koul et al., 2020). In the subsequent analysis, we investigate whether decadal trends corresponding to these three periods also emerge, after some years, in the regional environment of the Barents Sea.

A likely impact of the SPG on local oceanic conditions in the Barents Sea is implicitly hinted by the high correlation between the total stock biomass (TSB) of Northeast Arctic cod and SPG properties (**Figure 2** and **Table 1**). The TSB is the total biomass of mature and immature fish and it reflects the integrated impact of climate on fish population. The TSB time series suggests that the cod has undergone periods of decline and recovery, mainly at decadal to multi-decadal timescales (**Figure 2**). There is a statistically significant and high correlation between the TSB and SPG T/S (see **Table 1**), as was found in earlier investigations (Årthun et al., 2018; Koul et al., 2021). The correlation of TSB with surface salinity ($r = 0.82$) is similarly high as that with surface temperature ($r = 0.77$), which hints at a role of inflowing Atlantic Water into the Barents Sea. Read together with their advective lags, these high positive correlations point toward a possible impact of the SPG variability on cod biomass. As we show below, the SPG-driven changes in the Atlantic Inflow into the Barents Sea plays an important role.

The Atlantic Inflow mainly enters the Barents Sea through the BSO (see **Figure 1** for the location of this region). Before arriving at the BSO, the Atlantic Inflow crosses the Greenland-Scotland Ridge (Hátún et al., 2005) and passes through the FSC (Hansen et al., 2008). As illustrated in **Figure 1**, the core of Atlantic Inflow is seen as subsurface salinity maxima in the water column. Thus, the correlations of the SPG T and S are lower with respective surface T and S at the BSO than with sub-surface T and S (**Figure 3** and **Table 1**). Note that the correlations are calculated from linearly detrended time series. The decadal to multi-decadal variability, particularly the freshening of the BSO from 1970 to 1979 (corresponding to the freshening of the SPG in the late 1960s) clearly emerges in sub-surface salinity time series and to some extent in the corresponding decrease of the sub-surface temperature only. The lack of correlation of the surface T and S at the BSO with the SPG T and S together with pronounced interannual variability at the surface suggests a dominating impact of overlying atmospheric variability.

Another way to assess the impact of SPG on oceanic properties downstream of the Greenland-Scotland Ridge is through the variability in volume transport. The mean total volume transport (see Methods for the definition) is high at the FSC and relatively low at the BSO—the 1960–2019 mean volume transport is about 5.9 Sv at the FSC and 3.65 Sv at the BSO. Downstream of the FSC, the Atlantic Water mixes with ambient water masses and dilutes its properties. This is apparent in the maximum total volume transport which occurs at T = 9-10 °C and S = 35.3-35.4 at the FSC and at T = 6-7 °C and S = 35.0-35.1 at the BSO (**Figure 4**). The decadal to multi-decadal variability seen in the SPG is present in the Atlantic Inflow. The Atlantic Inflow (see Methods for the definition) through the FSC decreased during the cooling and freshening of the SPG in 1960s, the inflow increased during the warming and salinification of the SPG in mid 1990s, and the recent cooling of the SPG has coincided with ongoing reduction of the Atlantic Water (**Figure 4**).

The low frequency character of the Atlantic Inflow at the FSC is also largely seen in the Atlantic Inflow at the BSO ($r = 0.67$,

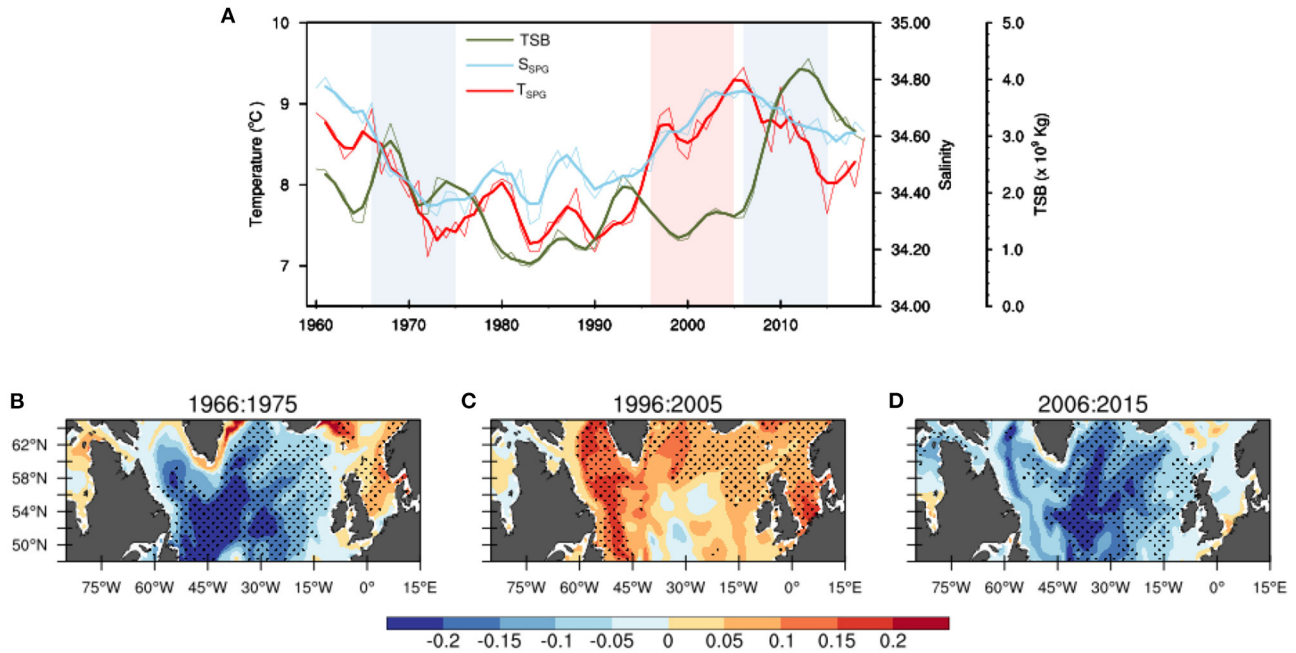

FIGURE 2 | (A). Time series of modelled surface temperature and surface salinity of the North Atlantic Subpolar Gyre (-60:-10 °E, 50:62 °N) from the assimilation experiment, and total stock biomass of cod in the Barents Sea for the period 1960–2019. For each of the time series shown, light lines are annual means and bold lines are three-year running mean values. The time series are not linearly detrended. The blue and red shaded time periods highlight the three dominant decadal trends. Trends in the surface temperature of the North Atlantic Subpolar Gyre (°C yr^{-1}) for **(B)** 1966–1975 cooling, **(C)** 1996–2005 warming, and **(D)** 2006–2015 cooling. The stippling marks statistically significant trends at 90% confidence level.

TABLE 1 | Pearson's correlation coefficients (r) among various variables and the lag at which r is maximum (@Lag (years)).

	TSB	*BSO T_{6m}*	*BSO T_{200m}*	*BSO S_{6m}*	*BSO S_{200m}*	*FSC Atl. Inflow*	*BSO Atl. Inflow*	*BS Aw Vol.*	*BS Sice. Ar.*
SPG T_{6m}	**0.77** @7	0.27 @4	0.38 @4	0.31 @4	**0.79** @4	**0.64** @3	**0.59** @4	x	x
SPG S_{6m}	**0.82** @7	0.22 @5	0.41 @4	0.22 @5	**0.76** @4	**0.57** @3	**0.56** @4	x	x
FSC Atl. Inflow	x	x	x	x	x	x	**0.67** @1	x	x
BSO Atl. Inflow	x	x	x	x	x	x	x	**0.80** @1	**-0.51** @1
BS Aw. Vol.	x	x	x	x	x	x	x	x	**-0.62** @0

The bold values are correlations that are significant at 95% confidence level.

lag = 1 year), and both have a statistically significant correlation with SPG T and S (**Table 1**). The variability in the Atlantic Inflow at the BSO is not closely linked with the wind stress curl over the Barents Sea (**Figure 4**). For the time period considered (1960–2019), the correlation between the wind stress curl and the Atlantic Inflow is low and statistically insignificant ($r = 0.25$, lag = 0 year). As is clear from the time series, the wind stress curl exhibits a strong interannual variability. However, wind stress curl drives the total volume transport at the BSO (r = -0.71, **Supplementary Figure 2**). Thus it appears that the warm and saline part of the total volume transport, i.e., the Atlantic Inflow, is related to the variability in the SPG. The respective correlations (**Table 1**) also suggest that the SPG signal is much clearer in the depth-integrated Atlantic Inflow than in temperatures at a single depth.

The volume of Atlantic Water within the Barents Sea (red box in **Figure 1**) shows a general increasing trend from the late 1970s (**Figure 5**). This is inline with the gradual Atlantification of the Barents Sea in the recent decades. The variability of Atlantic Water within the Barents Sea is directly related to the Atlantic Inflow at the BSO (r = 0.8, lag = 1 year, **Figure 5**). In the 1970s, a nearly 30% reduction in the volume of Atlantic Water in the Barents Sea occurred following the sharp decline in the Atlantic Inflow at the BSO during the same period (**Figure 5**). Similarly, Atlantic Water volume increased by about 20% from early 2000s following an increase in Atlantic Inflow. Interestingly, for the period 2010–2019 (corresponding to the most recent cooling/freshening of the SPG after accounting for the advective delays), while there was a decline in the Atlantic Inflow at the BSO (from a high of 1.5 Sv in 2010 to a low of 1.0 Sv in 2019), there was no significant change in the Atlantic Water volume during that period. Similarly, the variability in sea-ice area in the Barents Sea has closely followed the variability in both the Atlantic Inflow at the BSO and the volume of Atlantic Water in the Barents Sea

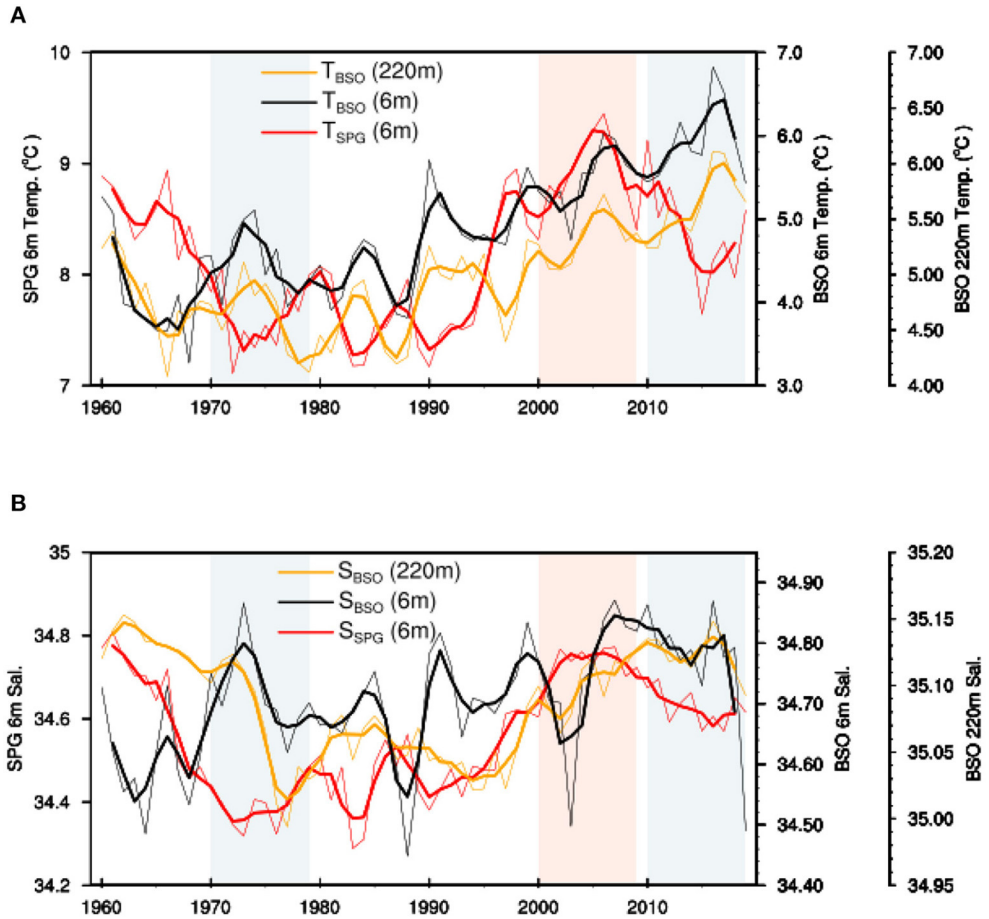

FIGURE 3 | Time series of modelled surface and sub-surface **(A)** temperature and **(B)** salinity in the North Atlantic Subpolar Gyre (-60:10 °E, 50:62 °N) and an the Barents Sea Opening (10:25 °E, 70:78 °N) for the period 1960–2019. For each of the time series shown, light lines are annual means and bold lines are three-year running mean values. The shaded time periods highlight the time periods four years after the respective decadal trends in the SPG.

(**Table 1**). Sea-ice in the Barents Sea grew in the 1970s, declined in the early 2000s and has not undergone a large decline from 2005 to 2019 in the assimilation experiment.

Differences in the spatial extent of the Atlantic Water within the Barents Sea present a more clearer picture of its regional inhomogeneities in Atlantic Water volume (**Figure 6**). Corresponding to the cooling/freshening in the 1970s, a reduction in the volume of Atlantic Water occurred in the southwestern region of the Barents Sea. Similarly, in the late 1990s and early 2000s when more Atlantic Water entered the Barents Sea, an increase in the Atlantic Water volume occurred as far as 35°E. Even for the last decade of our interest (2010–2019), a decline in the Atlantic Water volume has occurred which was not evident from the area integrated time series (**Figure 5**). Clearly, most of this decline is limited to the southwestern region of the Barents Sea from where the Atlantic Water enters the Barents Sea (i.e., along the mean current pathways). The location of the 1°C isotherm at 100 m, applied here as a proxy for the northern limit of the Atlantic Water, also presents a consistent picture, except for the last decade when the isotherm shifted further northward from 2010 to 2019.

Now, we turn to the key aspect of the impact of the SPG, i.e., the changes in the sea-ice extent and primary production in the Barents Sea. An increase in sea-ice area limits the available area for the primary production in the Barents Sea (Dalpadado et al., 2014), which can reduce the feeding grounds of fish communities (Drinkwater et al., 2010). Thus, an impact of SPG on sea-ice area and primary production in the Barents Sea may provide the physical explanation behind the high correlations between SPG and cod biomass (**Figure 2** and **Table 1**). After adjusting for advective delays inferred from preceding analysis, trends in sea-ice area fraction and primary production can be identified along the climatological sea-ice boundary (**Figure 7**). In the first two decades of interest (1971 to 1980 and 2001 to 2010), the trends are strongest in the northern Barents Sea along the sea-ice edge. The first cooling period results in the growth of sea-ice in the Barents Sea and a corresponding decline in the net primary production. Similarly, the 1990s warming of the SPG leads to a decline in the sea-ice area from 2001–2010 and a

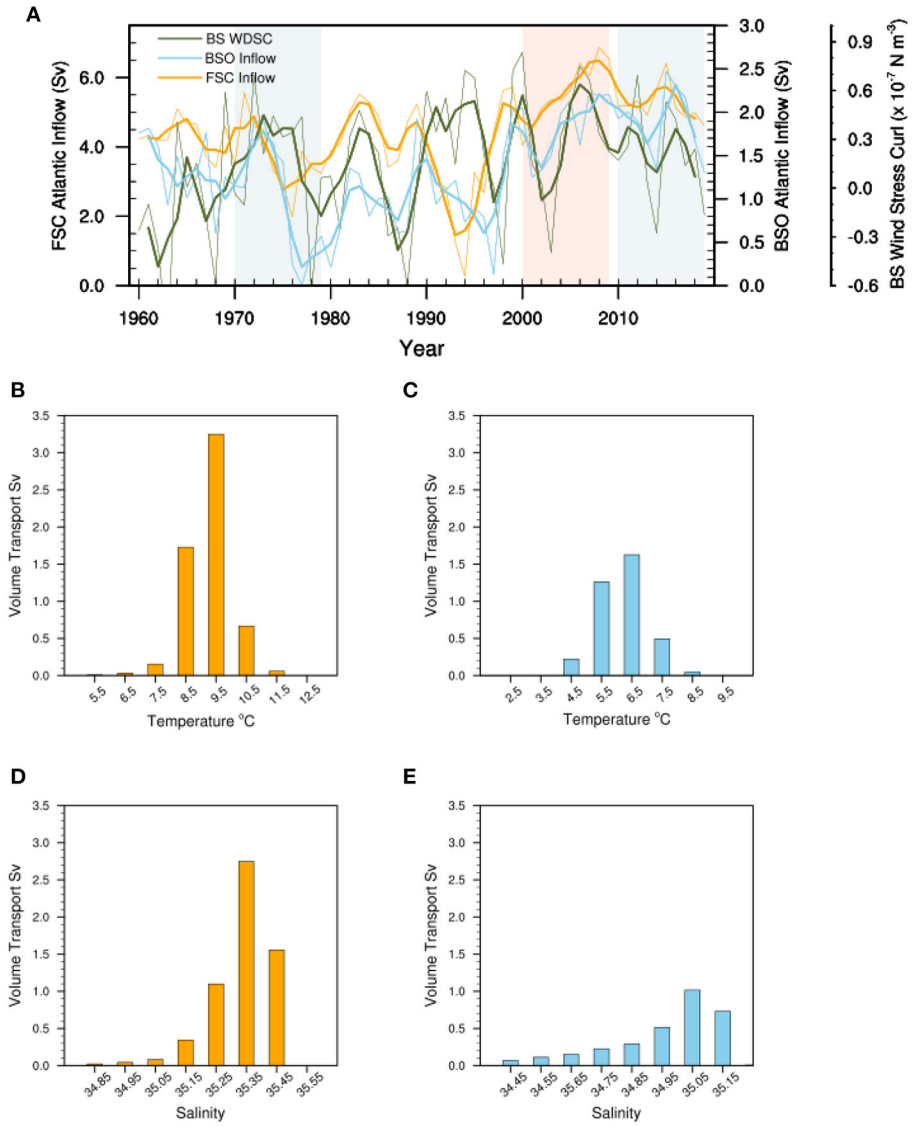

FIGURE 4 | (A) Time series of modelled Atlantic Inflow (Sv, 1 Sv = 10^6 m^3 s^{-1}) across the Faroe Scotland Channel (FSC, orange) and Barents Sea Opening (BSO, blue), and time series of wind stress curl (WDSC, green) over the Barents Sea (black box in **Figure 1A**). For each of the time series shown, light lines are annual means and bold lines are three-year running mean values. The shaded time periods highlight the time periods four years after the respective decadal trends in the SPG. Atlantic Inflow is defined as the volume transport of water with eastward zonal velocity and with T > 8.5 °C and S > 35.25 at the FSC, and T > 5.5 °C and S > 35.0 at the BSO. Histograms of volume transport (Sv) in various temperature (T) and Salinity (S) classes across the **(B,D)**, FSC and **(C,E)**, BSO, respectively. The location of the FSC and the BSO section for computing volume transports is shown in **Figure 1A**.

corresponding increase in primary production. For the period 2011 to 2019, corresponding to the 2006–2015 cooling of the SPG, the increase in the sea-ice area and the resulting decrease in primary production has occurred mainly outside and further north of the Barents Sea. Within the Barents Sea, however, a positive trend in the primary production emerges. This aspect is taken up further in the discussion section.

As we have not assimilated satellite observations into the model, it is instructive to see whether similar trends have emerged in satellite observations of sea-ice concentration and primary production (**Figure 8**). For the decade 2001 to 2010, the decadal trends in observed sea-ice concentration show a similar statistically significant decline as seen in the assimilation experiment. The sea-ice edge moved northwards in this decade owing to the increased heat transport into the Barents Sea. For the decade 2011 to 2020, although a statistically significant trend has not emerged in the Barents Sea, the absence of a declining trend in sea-ice is consistent with the antecedent cooling of the SPG. In the case of observed net primary production, the pronounced increase along the sea-ice edge in the decade when sea-ice retreated northwards, as was seen in the assimilation, is absent. However, in the last decade, 2011–2020, the decline

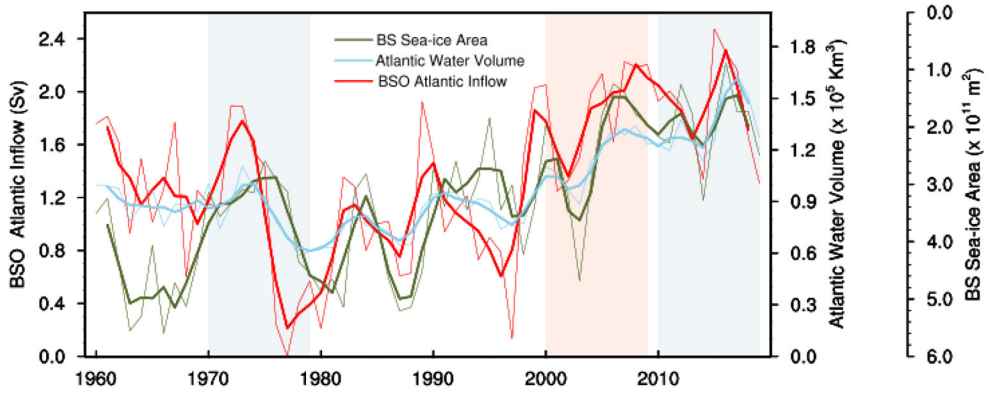

FIGURE 5 | Time series of modelled Atlantic Inflow (Sv) across the Barents Sea Opening (BSO, red), volume of Atlantic Water (Km^3) in the Barents Sea (blue) and total sea-ice area (m^2) in the Barents Sea (green). Following (Oziel et al., 2016), Atlantic Water is defined as water with T > 3.5 °C and S > 34.8 within the Barents Sea. For each of the time series shown, light lines are annual means and bold lines are three-year running mean values. The shaded time periods highlight the time periods four years after the respective decadal trends in the SPG.

within the Barents Sea is inline with reduced Atlantic Water volume (**Figure 6I**) but a statistically significant trend is yet to emerge.

In summary, our results reveal decadal changes in the marine environment of the Barents Sea that are related to the upstream changes in the subpolar North Atlantic. The SPG signal present in the Atlantic Inflow, both at the FSC and the BSO, is closely linked with the volume of Atlantic Water in the Barents Sea, which then has an impact on the sea-ice area and primary production, and consequently, on the cod biomass.

4. DISCUSSION AND CONCLUSIONS

In this article, through a data assimilation experiment, we present evidence to support the hypothesis that oceanic anomalies associated with the SPG have an impact on oceanic conditions in the Barents Sea. Recently, the Northeast Arctic cod biomass was shown to be predicable at multi-year lead times wherein a statistical temperature-cod relationship was leveraged (Årthun et al., 2018; Koul et al., 2021). Here, we present the mechanistic links underlying the statistical temperature-cod relationship, and we reveal SPG-driven co-variability in the Atlantic Inflow at the FSC and the BSO. Our results suggest that SPG-driven changes in the Atlantic Inflow are the primary drivers of decadal trends in the sea-ice area and primary production in the Barents Sea.

Our results, although derived in an Eulerian framework, corroborate the earlier reported 3–5 year advective delay in the propagation of oceanic anomalies from the eastern subpolar North Atlantic into the Barents Sea (Gao et al., 2005; Holliday et al., 2008; Langehaug et al., 2019). Our data assimilation based analysis also shows that the core of the warm and saline Atlantic Water lies at 150–300 m depth in the water column, both in the FSC and at the BSO, consistent with observations (Furevik, 2001; Yashayaev and Seidov, 2015). We find that the SPG signal is more pronounced in subsurface salinity downstream of the Greenland-Scotland Ridge (**Figure 3**). Temperature, due to air-sea interactions, has a short memory of the antecedent forcing history.

The dynamical basis of multiyear changes in volume transport of Atlantic Water into the Barents Sea, following periods of strong decadal trends in the SPG temperature and salinity, is the weakening and strengthening of the SPG circulation. The warming and cooling of the SPG is dynamically related to its weakening and strengthening, respectively (Bersch et al., 2007; Häkkinen et al., 2011; Koul et al., 2019, 2020). The strength of the SPG circulation controls the throughput of subtropical waters crossing the Greenland-Scotland Ridge. It is this SPG-driven waxing and waning of high salinity (and high temperature) waters that is mirrored in the Atlantic Inflow at decadal to multi-decadal timescales. At seasonal and interannual timescales, the SPG signal is contaminated by overlying atmospheric variability.

The interannual to decadal variability in the total volume transport is driven by the wind stress curl over the northern Barents Sea, however, the same is not the case for the Atlantic Inflow (**Supplementary Figure 2** and **Figure 4**). The low frequency variability as seen in Atlantic Inflow at BSO does not match that in the wind stress curl. This suggests that while the total volume transport is wind driven and is an important driver of the variability in sea-ice and primary production in the Barents Sea (Sandø et al., 2021), the warm and saline part of the total volume transport (i.e., the Atlantic Inflow) is instead driven by the variability in SPG-associated changes in temperature and salinity. Nevertheless, the large scale wind field over the subpolar North Atlantic plays an important role in the variability of the SPG circulation (Koul et al., 2020; Holliday et al., 2020).

It is possible that SPG-associated variability in temperature and salinity between the FSC and BSO might lead to local geostrophic circulation anomalies which can in turn influence Atlantic Inflow across the BSO. We do find consistent trends in temperature, salinity and zonal geostrophic currents in the first two decades of our analysis (**Supplementary Figure 3**),

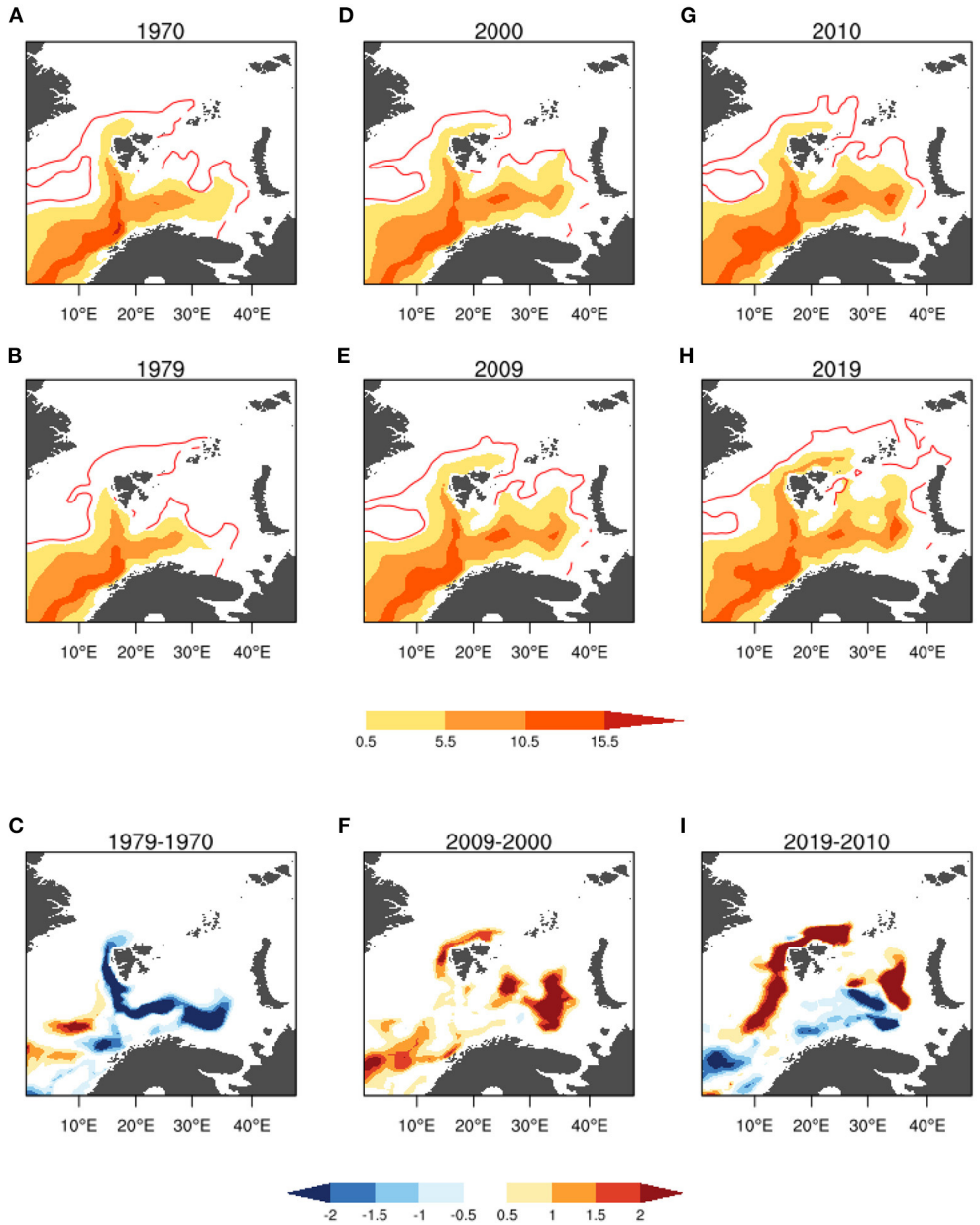

FIGURE 6 | Mean volume of Atlantic Water (x10^2 Km^3) at each grid point from the assimilation experiment over three years centered on **(A)** 1970, **(B)** 1979, their difference **(C)** 1979–1970, **(D)** 2000, **(E)** 2009 and their difference **(F)** 2009–2000. Since the model experiment ends at 2019, the Atlantic Water volume is shown for individual years **(G)** 2010, **(H)** 2019 and their difference **(I)** 2019–2010. The red contour line is the 1°C isotherm at 182 meters model level.

however, except salinity, the trends over the last decade show an inconsistent increase in both temperature and geostrophic currents. This can be due to the fact that in the last decade, the waters at the BSO have freshened and their temperatures have increased (**Figure 3**). This would cause a local steric sea level change resulting in anomalous eastward geostrophic flow. Noting that the trends are spatially incoherent, we leave it to future studies to quantify the impact of such geostrophic current anomalies on Barents Sea temperature and salinity.

Within the Barents Sea, observation show near doubling of the area occupied by the Atlantic Water over the last three to four decades (Oziel et al., 2016). In this article, we show that embedded in the long term trend are decadal changes in the area occupied by the Atlantic Water. In the first two decades analyzed in this study (i.e., 1970–1979 and 2000–2009), the extent of the area occupied by the Atlantic Water follows decadal trends in the SPG temperature, i.e., a decline in the former and an increase in the latter

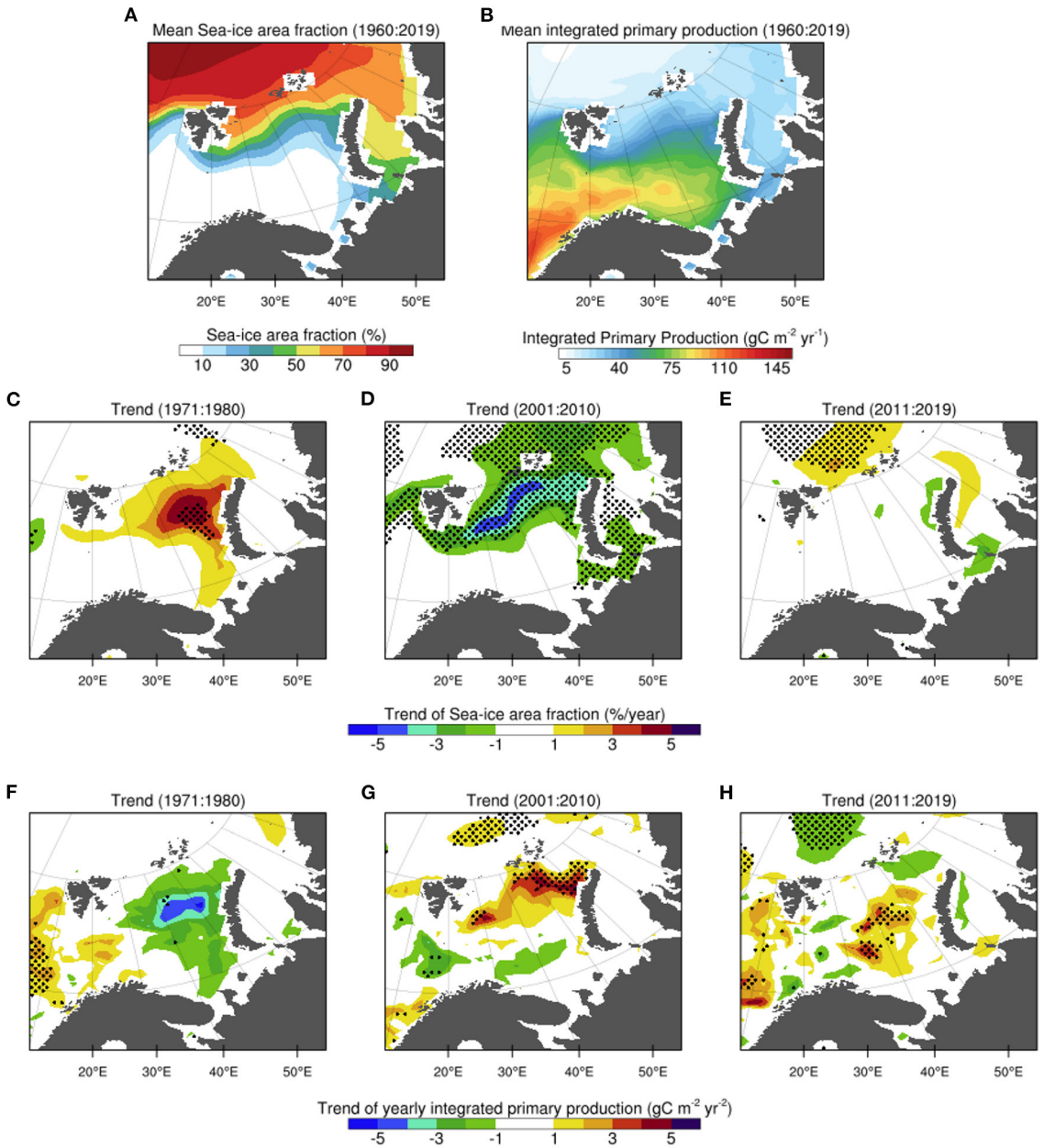

FIGURE 7 | (A) Climatology of the annual mean sea-ice concentration (percent of grid cell occupied by sea-ice) and **(B)** integrated net primary production ($gCm^{-2}yr^{-1}$) for the period 1960–2019 from the assimilation experiment. Trends in annual mean sea-ice concentration (second row) and integrated net primary production (third row) for the three periods **(C,F)** 1971–1980, **(D,G)** 2001–2010, and **(E,H)** 2011–2019. The stippling marks statistically significant trends at 90% confidence level.

decade. While this holds for the last period considered as well (2010–2019), the change is not uniform throughout the Barents Sea. The decline is mainly seen in the southwestern region from where the Atlantic Water enters the Barents Sea. Also, this decline is mainly due to a decrease in salinity than due to a decrease in temperature (**Figure 3** and **Supplementary Figure 3**). The analysis of the differences in Atlantic Water volume for the last decade is based on individual years (2019 and 2011) and thus might be contaminated by interannual variability. A clear signal might have emerged after 2019.

Sea-ice in the Barents Sea exerts a dominant control on the spatial distribution of primary production. Observations over a short record of less than 20 years suggest a bi-modal pattern in the spatial distribution of primary production which closely tracks the position of sea-ice edge during years with large changes

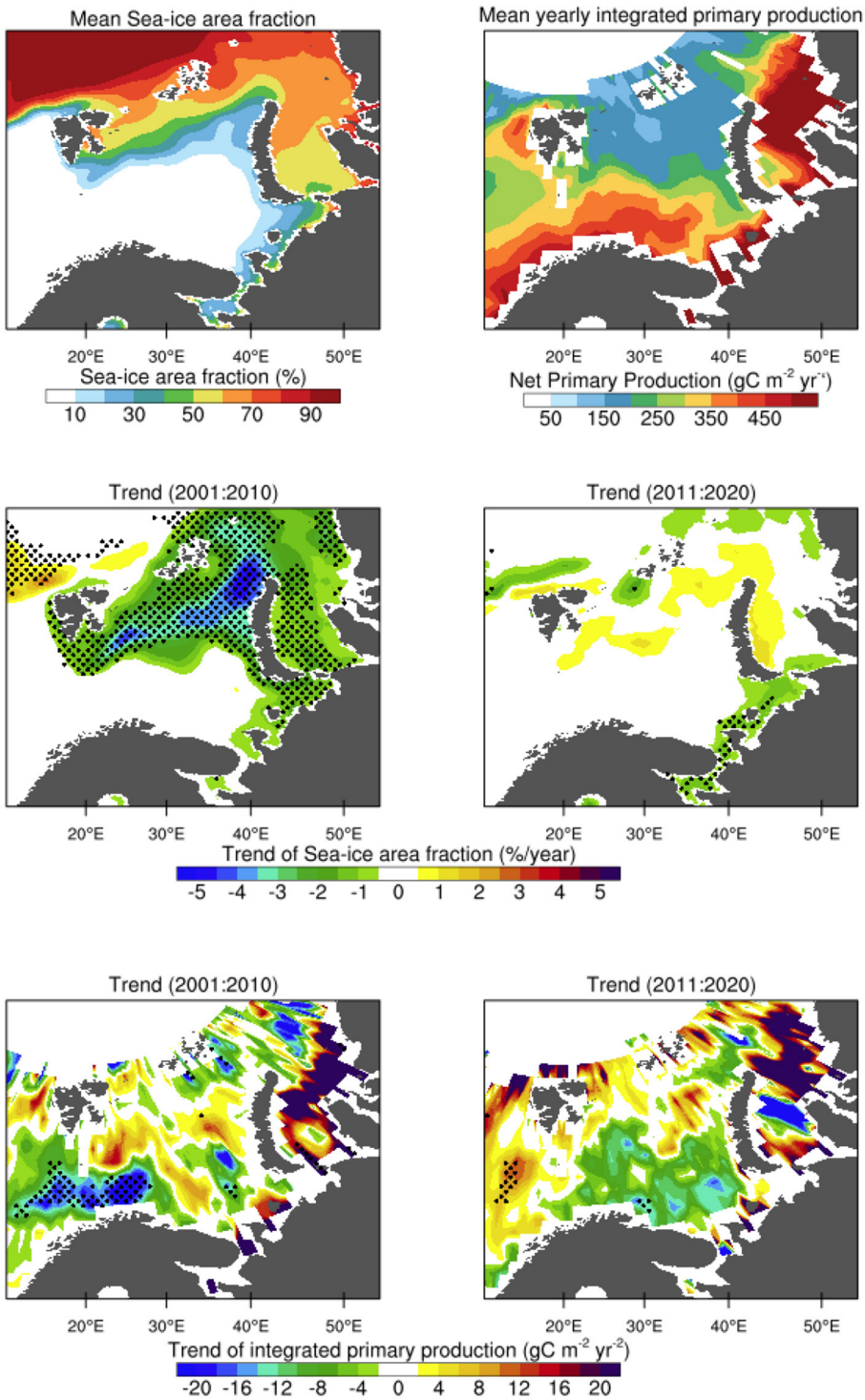

FIGURE 8 | Climatology of the annual mean sea-ice concentration and integrated net primary production ($gCm^{-2}yr^{-1}$) for the period 1997–2020 from satellite observations. Trends in annual mean sea-ice concentration (second row) and integrated net primary production (third row) for the two periods 2001–2010 and 2011–2020. The stippling marks statistically significant trends at 90% confidence level.

in sea-ice extent (Oziel et al., 2017). In our analysis, although we also find that the variability in the primary production closely tracks the sea-ice edge, the spatial pattern of the response of primary production to decadal changes in sea-ice extent is different. We find significant trends in primary production in response to trends in sea-ice area fraction both within and

outside the Barents Sea. For the period 2011–2019, significant increase in sea-ice and decrease in primary production has occurred north of Spitzbergen. This suggests that as the region of interaction between Atlantic Water and sea-ice shifts northward due to long term warming, the influence of the SPG would also extend northward.

Given the advective delays from the subpolar North Atlantic to the Barents Sea, the full impact of recent cooling of the SPG is expected after 2019, which is the last year of our experiment, and which could also explain the absence of significant trends in the northern Barents Sea in the last 9 years of our analysis. This latter conjecture is supported by the trends in the observed sea-ice and primary production for which the year 2020 is included. There is no significant declining trend in sea-ice concentration toward the north and the reduction in primary production is seen within the Barents Sea for the period 2011–2020. The absence of a decline in the sea-ice in the last decade of our analysis is consistent with the predicted slowdown of the sea-ice loss in the Barents Sea sector (Yeager et al., 2015) and satellite observations showing a slight recovery from the 2012 minimum.

The decadal trends in sea-ice and primary production, associated with the SPG, can influence cod biomass in various ways. For example, a large ice-free region allows habitat expansion which favours growth through increased food availability (Ottersen et al., 2010). A northward retreat of sea-ice edge also allows increased northward penetration of nutrients and zooplankton carried by the Atlantic Inflow, both of which can have an impact on the growth of Capelin, the main prey of cod in the Barents Sea. Thus, the high correlation between the SPG temperature, salinity and cod biomass is a manifestation of impact of the SPG on marine environment of the Barents Sea which has implications for predictability of marine ecosystems in this shelf-sea.

DATA AVAILABILITY STATEMENT

The raw data supporting the conclusions of this article will be made available by the authors, without undue reservation.

AUTHOR CONTRIBUTIONS

VK and CS conceived the work and discussed the research plan. VK analyzed the data, model experiments, prepared the figures, and wrote the manuscript. SB carried out model experiments. SB, JB, and CS discussed results, their interpretation, and helped with the improvement of the manuscript.

FUNDING

This study is a contribution to the Excellence Cluster CliCCS - Climate, Climatic Change, and Society at the University of Hamburg, funded by the DFG through Germany's Excellence Strategy EXC 2037 Project 390683824, (JB and CS). This study is also a contribution to the PoF IV Program Changing Earth Sustaining our Future, Topic 4 Coastal Transition Zones under Natural and Human Pressure of the Helmholtz Association. JB and CS were supported by Copernicus Climate Change Service, funded by the EU, under contract C3S-330.

ACKNOWLEDGMENTS

The authors thank the German Computing Center (DKRZ) for providing their computing resources.

SUPPLEMENTARY MATERIAL

The Supplementary Material for this article can be found online at: https://www.frontiersin.org/articles/10.3389/fmars.2021.778335/full#supplementary-material

REFERENCES

Ådlandsvik, B., and Loeng, H. (1991). A study of the climatic system in the barents sea. *Polar Res.* 10, 45–50. doi: 10.3402/polar.v10i1.6726

Årthun, M., Bogstad, B., Daewel, U., Keenlyside, N. S., Sandø, A. B., Schrum, C., et al. (2018). Climate based multi-year predictions of the barents sea cod stock. *PLoS One* 13:e0206319. doi: 10.1371/journal.pone.0206319

Årthun, M., and Eldevik, T. (2016). On anomalous ocean heat transport toward the arctic and associated climate predictability. *J. Clim.* 29, 689–704. doi: 10.1175/JCLI-D-15-0448.1

Årthun, M., Eldevik, T., Smedsrud, L., Skagseth, Ø., and Ingvaldsen, R. (2012). Quantifying the influence of atlantic heat on barents sea ice variability and retreat. *J. Clim.* 25, 4736–4743. doi: 10.1175/JCLI-D-11-00466.1

Årthun, M., Eldevik, T., and Smedsrud, L. H. (2019). The role of atlantic heat transport in future arctic winter sea ice loss. *J. Clim.* 32:3327–3341. doi: 10.1175/JCLI-D-18-0750.1

Asbjørnsen, H., Johnson, H. L., and Årthun, M. (2021). Variable nordic seas inflow linked to shifts in north atlantic circulation. *J. Clim.* 1–50. doi: 10.1175/JCLI-D-20-0917.1

Behrenfeld, M. J., and Falkowski, P. G. (1997). Photosynthetic rates derived from satellite-based chlorophyll concentration. *Limnol. Oceanography* 42, 1–20. doi: 10.4319/lo.1997.42.1.0001

Bersch, M., Yashayaev, I., and Koltermann, K. P. (2007). Recent changes of the thermohaline circulation in the subpolar north atlantic. *Ocean Dyn.* 57, 223–235. doi: 10.1007/s10236-007-0104-7

Berx, B., Hansen, B., Østerhus, S., Larsen, K., Sherwin, T., and Jochumsen, K. (2013). Combining in situ measurements and altimetry to estimate volume, heat and salt transport variability through the faroe–shetland channel. *Ocean Sci.* 9, 39–654. doi: 10.5194/os-9-639-2013

Böning, C. W., Scheinert, M., Dengg, J., Biastoch, A., and Funk, A. (2006). Decadal variability of subpolar gyre transport and its reverberation in the north atlantic overturning. *Geophys. Res. Lett.* 33. doi: 10.1029/2006GL026906

Born, A., and Mignot, J. (2012). Dynamics of decadal variability in the atlantic subpolar gyre: a stochastically forced oscillator. *Clim. Dyn.* 39, 461–474. doi: 10.1007/s00382-011-1180-4

Bretherton, C. S., Widmann, M., Dymnikov, V. P., Wallace, J. M., and Bladé, I. (1999). The effective number of spatial degrees of freedom of a time-varying field. *J. Clim.* 12, 1990–2009. doi: 10.1175/1520-0442(1999)012<1990:TENOSD>2.0.CO;2

Brune, S., and Baehr, J. (2020). Preserving the coupled atmosphere-ocean feedback in initializations of decadal climate predictions. *WIREs Clim. Change* 11:e637. doi: 10.1002/wcc.637

Brune, S., Nerger, L., and Baehr, J. (2015). Assimilation of oceanic observations in a global coupled earth system model with the seik filter. *Ocean Model.* 96, 254–264. doi: 10.1016/j.ocemod.2015.09.011

Dalpadado, P., Arrigo, K. R., Hjøllo, S. S., Rey, F., Ingvaldsen, R. B., Sperfeld, E., et al. (2014). Productivity in the barents sea-response to recent climate variability. *PLoS One* 9:e95273. doi: 10.1371/journal.pone.0095273

Dalpadado, P., Ingvaldsen, R. B., Stige, L. C., Bogstad, B., Knutsen, T., Ottersen, G., et al. (2012). Climate effects on barents sea ecosystem dynamics. *ICES J. Marine Sci.* 69, 1303–1316. doi: 10.1093/icesjms/fss063

Dee, D. P., Uppala, S., Simmons, A., Berrisford, P., Poli, P., Kobayashi, S., et al. (2011). The era-interim reanalysis: Configuration and performance of the data assimilation system. *Quart. J. Roy. Meteorol. Soc.* 137, 553–597. doi: 10.1002/qj.828

Delworth, T., Manabe, S., and Stouffer, R. J. (1993). Interdecadal variations of the thermohaline circulation in a coupled ocean-atmosphere model. *J. Clim.* 6, 1993–2011. doi: 10.1175/1520-0442(1993)006<1993:IVOTTC>2.0.CO;2

Dickson, R. R., Meincke, J., Malmberg, S.-A., and Lee, A. J. (1988). The great salinity anomaly in the northern north atlantic 1968–1982. *Progr. Oceanography* 20, 103–151. doi: 10.1016/0079-6611(88)90049-3

Drinkwater, K. F., Beaugrand, G., Kaeriyama, M., Kim, S., Ottersen, G., Perry, R. I., et al. (2010). On the processes linking climate to ecosystem changes. *J. Marine Syst.* 79, 374–388. doi: 10.1016/j.jmarsys.2008.12.014

Drinkwater, K. F., Belgrano, A., Borja, A., Conversi, A., Edwards, M., Greene, C. H., et al. (2003). The response of marine ecosystems to climate variability associated with the north atlantic oscillation. *Geophys. Monograph Amer. Geophys. Union* 134, 211–234. doi: 10.1029/134GM10

Eyring, V., Bony, S., Meehl, G. A., Senior, C. A., Stevens, B., Stouffer, R. J., et al. (2016). Overview of the coupled model intercomparison project phase 6 (cmip6) experimental design and organization. *Geosci. Model Develop.* 9, 1937–1958. doi: 10.5194/gmd-9-1937-2016

Fossheim, M., Primicerio, R., Johannesen, E., Ingvaldsen, R. B., Aschan, M. M., and Dolgov, A. V. (2015). Recent warming leads to a rapid borealization of fish communities in the arctic. *Nat. Clim. Change* 5, 673–677. doi: 10.1038/nclimate2647

Furevik, T. (2001). Annual and interannual variability of atlantic water temperatures in the norwegian and barents seas: 1980–1996. *Deep Sea Res. Part I Oceanograph. Res. Papers* 48, 383–404. doi: 10.1016/S0967-0637(00)00050-9

Gao, Y., Drange, H., Bentsen, M., and Johannessen, O. M. (2005). Tracer-derived transit time of the waters in the eastern nordic seas. *Tellus B Chem. Phys. Meteorol.* 57, 332–340. doi: 10.3402/tellusb.v57i4.16553

Gent, P. R., Willebrand, J., McDougall, T. J., and McWilliams, J. C. (1995). Parameterizing eddy-induced tracer transports in ocean circulation models. *J. Phys. Oceanography* 25, 463–474. doi: 10.1175/1520-0485(1995)025<0463:PEITTI>2.0.CO;2

Glessmer, M. S., Eldevik, T., Våge, K., Nilsen, J. E. Ø., and Behrens, E. (2014). Atlantic origin of observed and modelled freshwater anomalies in the nordic seas. *Nat. Geosci.* 7, 801–805. doi: 10.1038/ngeo2259

Good, S. A., Martin, M. J., and Rayner, N. A. (2013). En4: Quality controlled ocean temperature and salinity profiles and monthly objective analyses with uncertainty estimates. *J. Geophys. Res. Oceans* 118, 6704–6716. doi: 10.1002/2013JC009067

Hagemann, S., and Gates, L. D. (2003). Improving a subgrid runoff parameterization scheme for climate models by the use of high resolution data derived from satellite observations. *Clim. Dyn.* 21, 349–359. doi: 10.1007/s00382-003-0349-x

Häkkinen, S., Rhines, P. B., and Worthen, D. L. (2011). Warm and saline events embedded in the meridional circulation of the northern north atlantic. *J. Geophys. Res. Oceans* 116. doi: 10.1029/2010JC006275

Hansen, B., Østerhus, S., Turrell, W. R., Jónsson, S., Valdimarsson, H., Hátún, H., et al. (2008). "The inflow of atlantic water, heat, and salt to the nordic seas across the greenland–scotland ridge," in *Arctic–Subarctic Ocean Fluxes* (Dordrecht: Springer), 15–43.

Hátún, H., Lohmann, K., Matei, D., Jungclaus, J. H., Pacariz, S., Bersch, M., et al. (2016). An inflated subpolar gyre blows life toward the northeastern atlantic. *Progr. Oceanography* 147, 49–66. doi: 10.1016/j.pocean.2016.07.009

Hátún, H., Payne, M., Beaugrand, G., Reid, P., Sandø, A., Drange, H., et al. (2009). Large bio-geographical shifts in the north-eastern atlantic ocean: From the subpolar gyre, via plankton, to blue whiting and pilot whales. *Progr. Oceanography* 80, 149–162. doi: 10.1016/j.pocean.2009.03.001

Hátún, H., Sandø, A. B., Drange, H., Hansen, B., and Valdimarsson, H. (2005). Influence of the atlantic subpolar gyre on the thermohaline circulation. *Science* 309, 1841–1844. doi: 10.1126/science.1114777

Holliday, N. P., Bersch, M., Berx, B., Chafik, L., Cunningham, S., Florindo-López, C., et al. (2020). Ocean circulation causes the largest freshening event for 120 years in eastern subpolar north atlantic. *Nat. Commun.* 11, 1–15. doi: 10.1038/s41467-020-14474-y

Holliday, N. P., Hughes, S., Bacon, S., Beszczynska-Möller, A., Hansen, B., Lavin, A., et al. (2008). Reversal of the 1960s to 1990s freshening trend in the northeast north atlantic and nordic seas. *Geophys. Res. Lett.* 35. doi: 10.1029/2007GL032675

Ilıcak, M., Drange, H., Wang, Q., Gerdes, R., Aksenov, Y., Bailey, D., et al. (2016). An assessment of the arctic ocean in a suite of interannual core-ii simulations. part iii: hydrography and fluxes. *Ocean Model.* 100:, 141–161. doi: 10.1016/j.ocemod.2016.02.004

Ilyina, T., Six, K. D., Segschneider, J., Maier-Reimer, E., Li, H., and Núñez-Riboni, I. (2013). Global ocean biogeochemistry model hamocc: Model architecture and performance as component of the mpi-earth system model in different cmip5 experimental realizations. *J. Adv. Model. Earth Syst.* 5, 287–315. doi: 10.1002/jame.20017

Ingvaldsen, R., Loeng, H., Ottersen, G., and Ådlandsvik, B. (2003). "Climate variability in the barents sea during the 20th century with focus on the 1990s," in *ICES Marine Science Symposia*, Vol. 219, 160–168.

Jungclaus, J., Fischer, N., Haak, H., Lohmann, K., Marotzke, J., Matei, D., et al. (2013). Characteristics of the ocean simulations in the max planck institute ocean model (mpiom) the ocean component of the mpi-earth system model. *J. Adv. Model. Earth Syst.* 5, 422–446. doi: 10.1002/jame.20023

Koul, V., Schrum, C., Düsterhus, A., and Baehr, J. (2019). Atlantic inflow to the north sea modulated by the subpolar gyre in a historical simulation with mpi-esm. *J. Geophys. Res. Oceans* 124, 1807–1826. doi: 10.1029/2018JC014738

Koul, V., Sguotti, C., Årthun, M., Brune, S., Düsterhus, A., Bogstad, B., et al. (2021). Skilful prediction of cod stocks in the north and barents sea a decade in advance. *Commun. Earth Environ.* 2, 140. doi: 10.1038/s43247-021-00207-6

Koul, V., Tesdal, J.-E., Bersch, M., Hátún, H., Brune, S., Borchert, L., et al. (2020). Unraveling the choice of the north atlantic subpolar gyre index. *Sci. Rep.* 10, 1–12. doi: 10.1038/s41598-020-57790-5

Langehaug, H. R., Sandø, A. B., Årthun, M., and Ilıcak, M. (2019). Variability along the atlantic water pathway in the forced norwegian earth system model. *Clim. Dyn.* 52, 1211–1230. doi: 10.1007/s00382-018-4184-5

Levitus, S., Matishov, G., Seidov, D., and Smolyar, I. (2009). Barents sea multidecadal variability. *Geophys. Res. Lett.* 36. doi: 10.1029/2009GL039847

Lien, V. S., Schlichtholz, P., Skagseth, Ø., and Vikebø, F. B. (2017). Wind-driven atlantic water flow as a direct mode for reduced barents sea ice cover. *J. Clim.* 30, 803–812. doi: 10.1175/JCLI-D-16-0025.1

Marshall, J., Johnson, H., and Goodman, J. (2001). A study of the interaction of the north atlantic oscillation with ocean circulation. *J. Clim.* 14, 1399–1421. doi: 10.1175/1520-0442(2001)014<1399:ASOTIO>2.0.CO;2

Marsland, S. J., Haak, H., Jungclaus, J. H., Latif, M., and Röske, F. (2003). The max-planck-institute global ocean/sea ice model with orthogonal curvilinear coordinates. *Ocean Model.* 5, 91–127. doi: 10.1016/S1463-5003(02)00015-X

Meier, W. N., F. Fetterer, A. K. Windnagel, and J. S. Stewart. (2021). *NOAA/NSIDC Climate Data Record of Passive Microwave Sea Ice Concentration, Version 4.* Boulder, CO: National Snow and Ice Data Center (NSIDC). doi: 10.7265/efmz-2t65

Muilwijk, M., Smedsrud, L. H., Ilicak, M., and Drange, H. (2018). Atlantic water heat transport variability in the 20th century arctic ocean from a global ocean model and observations. *J. Geophys. Res. Oceans* 123, 8159–8179. doi: 10.1029/2018JC014327

Orvik, K. A., and Skagseth, Ø. (2003). The impact of the wind stress curl in the north atlantic on the atlantic inflow to the norwegian sea toward the arctic. *Geophys. Res. Lett.* 30. doi: 10.1029/2003GL017932

Ottersen, G., Kim, S., Huse, G., Polovina, J. J., and Stenseth, N. C. (2010). Major pathways by which climate may force marine fish populations. *J. Marine Syst.* 79, 343–360. doi: 10.1016/j.jmarsys.2008.12.013

Ottersen, G., and Stenseth, N. C. (2001). Atlantic climate governs oceanographic and ecological variability in the barents sea. *Limnol. Oceanography* 46, 1774–1780. doi: 10.4319/lo.2001.46.7.1774

Oziel, L., Neukermans, G., Ardyna, M., Lancelot, C., Tison, J.-L., Wassmann, P., et al. (2017). Role for atlantic inflows and sea ice loss on shifting phytoplankton blooms in the b arents s ea. *J. Geophys. Res. Oceans* 122, 5121–5139. doi: 10.1002/2016JC012582

Oziel, L., Sirven, J., and Gascard, J.-C. (2016). The barents sea frontal zones and water masses variability (1980–2011). *Ocean Sci.* 12, 169–184. doi: 10.5194/os-12-169-2016

Pacanowski, R., and Philander, S. (1981). Parameterization of vertical mixing in numerical models of tropical oceans. *J. Phys. Oceanography* 11, 1443–1451. doi: 10.1175/1520-0485(1981)011<1443:POVMIN>2.0.CO;2

Piecuch, C. G., Ponte, R. M., Little, C. M., Buckley, M. W., and Fukumori, I. (2017). Mechanisms underlying recent decadal changes in subpolar north atlantic ocean heat content. *J. Geophys. Res. Oceans* 122, 7181–7197. doi: 10.1002/2017JC012845

Reick, C., Raddatz, T., Brovkin, V., and Gayler, V. (2013). Representation of natural and anthropogenic land cover change in mpi-esm. *J. Adv. Model. Earth Syst.* 5, 459–482. doi: 10.1002/jame.20022

Reverdin, G. (2010). North atlantic subpolar gyre surface variability (1895–2009). *J. Clim.* 23, 4571–4584. doi: 10.1175/2010JCLI3493.1

Robson, J., Ortega, P., and Sutton, R. (2016). A reversal of climatic trends in the north atlantic since 2005. *Nat. Geosci.* 9, 513–517. doi: 10.1038/ngeo2727

Sandø, A. B., Mousing, E. A., Budgell, W., Hjøllo, S. S., Skogen, M. D., and Ådlandsvik, B. (2021). Barents sea plankton production and controlling factors in a fluctuating climate. *ICES J. Marine Sci.* 78, 1999–2016. doi: 10.1093/icesjms/fsab067

Sandø, A. B., Nilsen, J. Ø., Gao, Y., and Lohmann, K. (2010). Importance of heat transport and local air-sea heat fluxes for barents sea climate variability. *J. Geophys. Res. Oceans* 115. doi: 10.1029/2009JC005884

Skagseth, Ø., Furevik, T., Ingvaldsen, R., Loeng, H., Mork, K. A., Orvik, K. A., et al. (2008). "Volume and heat transports to the arctic ocean via the norwegian and barents seas," in *Arctic–Subarctic Ocean Fluxes* (Springer), 45–64.

Smedsrud, L. H., Esau, I., Ingvaldsen, R. B., Eldevik, T., Haugan, P. M., Li, C., et al. (2013). The role of the barents sea in the arctic climate system. *Rev. Geophys.* 51, 415–449. doi: 10.1002/rog.20017

Smedsrud, L. H., Ingvaldsen, R., Nilsen, J., and Skagseth, Ø. (2010). Heat in the barents sea: Transport, storage, and surface fluxes. *Ocean Sci.* 6, 219–234. doi: 10.5194/os-6-219-2010

Stevens, B., Giorgetta, M., Esch, M., Mauritsen, T., Crueger, T., Rast, S., et al. (2013). Atmospheric component of the mpi-m earth system model: Echam6. *J. Adv. Model. Earth Syst.* 5, 146–172. doi: 10.1002/jame.20015

Yashayaev, I., and Seidov, D. (2015). The role of the atlantic water in multidecadal ocean variability in the nordic and barents seas. *Progr. Oceanography* 132, 68–127. doi: 10.1016/j.pocean.2014.11.009

Yeager, S. G., Karspeck, A. R., and Danabasoglu, G. (2015). Predicted slowdown in the rate of atlantic sea ice loss. *Geophys. Res. Lett.* 42, 10–704. doi: 10.1002/2015GL065364

Conflict of Interest: The authors declare that the research was conducted in the absence of any commercial or financial relationships that could be construed as a potential conflict of interest.

Publisher's Note: All claims expressed in this article are solely those of the authors and do not necessarily represent those of their affiliated organizations, or those of the publisher, the editors and the reviewers. Any product that may be evaluated in this article, or claim that may be made by its manufacturer, is not guaranteed or endorsed by the publisher.